

# A Numerical Optimization Study on Winglets

Shahriar Khosravi\* and David W. Zingg†

*Institute for Aerospace Studies, University of Toronto*

*4925 Dufferin Street, Toronto, Ontario, M3H 5T6, Canada*

This paper focuses on aerostructural optimization of wings with winglets. A Newton-Krylov flow solver for the Euler equations is interfaced with a finite-element structures solver for the aerostructural solution. A gradient-based optimizer is used for optimization, where gradients are calculated by the coupled discrete-adjoint method. Pareto fronts of optimal solutions are constructed for weight and drag, which are competing objectives in the context of wing design. Three winglet configurations are considered: winglet-up, winglet-down, and raked wingtips. These are compared to optimized planar wings of the same span. The aerostructural optimization cases reveal that the winglet-down configuration provides the largest benefit in comparison to the optimized planar wings by increasing the span of the wing at the deflected state.

## Nomenclature

$x, y, z$	Streamwise, spanwise, and vertical coordinates
$g$	Gravitational acceleration constant
$L$	Lift
$C_L$	Lift coefficient
$D$	Inviscid drag
$C_{D_i}$	Inviscid drag coefficient
$C_D$	Drag coefficient
$M$	Freestream Mach number
$\alpha$	Angle of attack
$C_p$	Pressure coefficient
$R$	Range indicator
$W$	Wing weight
$W_i$	Initial aircraft weight
$W_f$	Final aircraft weight
$t$	Thickness of structural components
$\beta$	Objective function parameter
$e$	Span efficiency factor from linear aerodynamic theory
$b$	Wing span
$q_\infty$	Dynamic pressure

## I. Introduction

THE rising cost of oil and increasing carbon emissions endanger the future of commercial aviation. If the airline industry is to maintain its growth, commercial airplanes must become highly efficient in terms of fuel consumption. As a result, drag reduction is an important area of research in aviation because aircraft fuel consumption is directly related to drag.

---

\*Ph.D. Candidate, AIAA Student Member, shahriar.khosravi@mail.utoronto.ca

†Professor and Director, Canada Research Chair in Computational Aerodynamics and Environmentally Friendly Aircraft Design, J. Armand Bombardier Foundation Chair in Aerospace Flight, Associate Fellow AIAA, dwz@oddjob.utias.utoronto.ca

Lift-induced drag (or more simply induced drag) is typically 40% of the total drag of a commercial aircraft in cruise.<sup>1</sup> It is therefore worthwhile to explore concepts that reduce the induced drag. This has been the primary motivation for researchers to study nonplanar wings and, in particular, winglets. There have been many studies in the past decades on the possible fuel efficiency improvements provided by winglets. We mention a few important examples in this paper; a more thorough review is provided by Kroo.<sup>1</sup>

The term *winglet* was first used by Whitcomb<sup>2</sup> at NASA. He showed that winglets can provide a significant improvement in the lift-to-drag ratio over planar wingtip extensions at the same level of root bending moment. While the winglets and wingtip extensions were designed by a combination of available theory and wind tunnel tests, the wing itself was not redesigned. At the same time, another study done by NASA considered the relative advantages of winglets and wingtip extensions.<sup>3</sup> It concluded that at the same level of root bending moment, winglets provide a greater induced drag reduction than a wingtip extension. Later, another study by Jones and Lasinsky<sup>4</sup> concluded that when optimized wing shapes are considered, similar reductions of induced drag may be achieved either by extending the wingtip or by having a vertical winglet.

Asai<sup>5</sup> studied the relative advantages of planar and nonplanar wings and concluded that the tradeoff between the induced drag and wing root bending moment alone is not enough to determine the effectiveness of winglets. The effects of the viscous drag penalty incurred by winglets must also be taken into account. He further suggested that if both the root bending moment and viscous drag are kept constant, it is possible to design a planar wing with lower total drag than any nonplanar wing. Van Dam<sup>6</sup> considered planar wings that produce a nonplanar wake at a nonzero angle of attack and suggested that these geometries can provide considerable induced drag reductions. However, much of the improvement was later attributed to numerical integration inaccuracies.<sup>7</sup>

More recently, Takenaka and Hatanaka<sup>8</sup> performed a multidisciplinary design exploration for a winglet using high-fidelity computational fluid dynamics (CFD) and computational structural mechanics. They considered a sample of 32 winglets having various root chord lengths, taper ratios, sweep angles, spans, cant angles, and toe angles for multidisciplinary design optimization (MDO) based on the Kriging model. Their optimized winglet provides a reduction in total drag of approximately 22 drag counts while increasing the wing root bending moment by 5.3%. Furthermore, they demonstrated that a conventional winglet, one that is a vertical extension of the wingtip geometry, can only provide a reduction of 17 drag counts while increasing the root bending moment by 3.5% in comparison to the baseline planar wing. The total drag reductions provided by the wings with winglets were also validated using wind tunnel tests. However, it is important to note that only the winglets were optimized in this study. The shape of the wing was not optimized.

Another notable numerical study, done by Verstraeten and Slingerland,<sup>9</sup> focused on the drag characteristics of optimally loaded planar wings, wings with winglets, and c-wings using a low-fidelity model of the aerodynamics and weight. They concluded that when a span constraint exists, a wingletted wing with a height-to-span ratio of 28% provides a total drag reduction of 5.4% in comparison to a planar wing at identical wing root bending moments. This study also demonstrated that winglets can be used to provide induced drag reductions when there is a constraint on the aspect ratio of the wing. Ning and Kroo<sup>10</sup> did a similar study, but included the area-dependent weight in their calculations too. They also took into account the effects of a critical structural load factor on the tradeoffs in the design of wings with winglets. Another notable difference in this study was the inclusion of a stall speed constraint. They demonstrated that whether a winglet performs better than a wingtip extension depends on the ratio of the maneuver lift coefficient to the cruise lift coefficient. At the cruise load condition, a wingtip extension is slightly more advantageous while the winglet performs marginally better when a 2.5g critical load condition is considered. This trend held true for both retrofits and new wing designs.

Using a medium-fidelity aerostructural optimization approach, Jansen et al.<sup>11</sup> showed that a wing with a winglet is the optimal design when a span constraint exists. Furthermore, when the span is unconstrained, the optimal design is a raked wingtip. This work was followed by a notable study by Hicken and Zingg.<sup>12</sup> They performed high-fidelity aerodynamic shape optimization based on the Euler equations for several nonplanar geometries. This study showed that a winglet-up configuration with a height-to-span ratio of 10% can provide an induced drag reduction of approximately 15% for a low-speed, rectangular, and unswept

wing. The span and the planform area of the two wings were kept constant in this study, while the surface area of the nonplanar wing was 10% greater than the planar wing. Gagnon and Zingg<sup>13</sup> later performed high-fidelity aerodynamic shape optimization for several aircraft configurations and showed that a canted winglet can reduce the induced drag of a transonic conventional wing by 3.5%.

Despite all of the research effort on this subject, there is still no clear answer as to whether or not nonplanar wingtips can be used to provide significant fuel efficiency improvements, especially for a new wing design. Conclusions made in the past vary depending on the specific design problem considered and the level of physical detail that the models used are able to capture. This means that more work needs to be done in order to understand the fundamental tradeoffs in the design of wings with winglets. The present study attempts to contribute to this objective through the application of high-fidelity aerostructural optimization, where the deflections of the wing are taken into account and the aerodynamic and structural optimizations are fully coupled. It is important to note that we consider only new wing designs in this study, as opposed to retrofits.

## II. Methodology

The aerostructural optimization framework used in this work consists of five main components: 1) a multi-block Newton-Krylov-Schur flow solver for the Euler and Reynolds-Averaged-Navier-Stokes equations,<sup>14,15</sup> 2) a finite-element structural solver for the analysis and optimization of the structure,<sup>16</sup> 3) an algebraic grid movement algorithm for moving the CFD grid during optimization,<sup>17</sup> 4) a free-form deformation (FFD) method for geometry parameterization,<sup>18</sup> and 5) the gradient-based optimizer SNOPT<sup>19,20</sup> with gradients calculated using the discrete-adjoint method for the coupled multidisciplinary system. Since the two discipline solvers are written in different programming languages, we use Python to provide an interface for the solvers. This framework is largely based on the work of Kenway et al.<sup>21</sup> Details are outlined in Leung et al.<sup>22</sup>

The flow solver is based on an efficient multiblock finite-difference methodology that makes use of summation-by-parts operators for the spatial discretization and simultaneous approximation terms for the imposition of block boundary and interface conditions. The solution to the discrete equations at each Newton step is computed using the generalized minimum residual scheme with approximate Schur preconditioning. The one-equation Spalart-Allmaras turbulence model is used to model turbulent flows. All the optimization results presented in this paper are based on the Euler equations. Hicken and Zingg<sup>14</sup> and Osusky and Zingg<sup>15</sup> provide comprehensive details of the flow solver.

The structural analysis is performed by a parallel finite-element code called the Toolkit for the Analysis of Composite Structures (TACS).<sup>16</sup> It is capable of performing either linear or geometrically nonlinear analysis. However, only linear analysis is considered in this study. TACS is able to handle all of the required design variables for the thickness values of structural components inside the wing box. It is written in C++ and provides a Python interface for straightforward coupling to solvers from other disciplines. Additionally, it has the built-in capability to provide sensitivities with respect to the design variables.

Performing aerostructural analysis and optimization requires transferring the loads and displacements between the aerodynamic and structural solvers. To accomplish this goal, rigid links are constructed between the aerodynamic surface nodes, where the aerodynamic forces are calculated, and the closest points on the structures finite-element mesh. The displacements are then extrapolated from the structures mesh to the CFD surface.<sup>16</sup> The main advantages of this scheme are that it is consistent and conservative, and it is able to transfer loads and displacements between aerodynamic and structures meshes that are not coincident.

We use an FFD approach for the manipulation of the geometry, as outlined by Kenway et al.<sup>18</sup> In this method, both the CFD surface mesh and the structures finite-element mesh are embedded inside a B-spline FFD volume. The control points of the FFD volume may then be manipulated by the optimizer to make modifications to the geometry. The control points can also be grouped to define global planform variables.

A gradient-based optimizer is used for optimization because gradient-based optimizers typically require fewer function evaluations than genetic algorithms.<sup>23</sup> Using a gradient-based optimizer means that only a

local optimum can be found. However, Chernukhin and Zingg<sup>24</sup> have proposed gradient-based global optimization strategies that can be used to address this issue. The gradients of the objective and constraints are computed using the coupled adjoint method outlined by Martins et al.<sup>25</sup> This is an efficient method for problems with many more design variables than constraints because the cost of computing the gradient is nearly independent of the number of design variables. We use the gradient-based sequential quadratic programming optimization algorithm SNOPT, which allows for the solution of large-scale constrained problems.<sup>19</sup> PyOpt<sup>20</sup> is used to provide a Python interface for SNOPT.

### III. Results

This section presents the results from optimization cases performed using the framework described above. A family of objective functions is considered where the sum of normalized inviscid drag and normalized weight of the wing is minimized with varying emphasis on drag and weight. The goal is to construct Pareto fronts of optimal solutions for drag and weight, which are competing objectives in the context of wing design, and compare them for wingletted and planar wings. We consider three winglet configurations: winglet-up, winglet-down, and raked wingtips. We also assume that the span is constrained by an airport operating requirement.

The baseline wing geometry for this study is loosely based on a Boeing 737-900 wing with the RAE 2822 supercritical airfoil. All of the winglet configurations that are considered have the same undeflected span as the baseline wing and, as a result, have the same planform area as the baseline wing. The projected span of the wing, however, may change due to the structural deflection of the wing. There are two operating conditions: cruise and 2.5*g* pull-up maneuver. The cruise condition is  $M = 0.74$  at an altitude of 30,000 ft while the maneuver condition is  $M = 0.85$  at an altitude of 20,000 ft. The 2.5*g* load condition is determined based on Kroo’s methodology.<sup>26</sup> More details about the maneuver load condition are provided in Subsection B.

#### A. Objective Function

The choice of the objective function significantly influences the final optimized design. For practical design of wings, the objective is carefully chosen based on the operating requirements for a particular aircraft. However, our main goal in this study is not to discover the best wing for a particular commercial airplane. Instead, we are interested in the fundamental tradeoffs between drag and weight that are involved in the design of wings with winglets. For this reason, we choose an objective function of the form

$$J = \beta \frac{D}{D_0} + (1 - \beta) \frac{W}{W_0} \quad (1)$$

where  $\beta$  is a parameter between zero and unity,  $D$  is the inviscid drag of the wing in cruise,  $W$  is the calculated weight of the wing satisfying the structural failure constraints at the 2.5*g* load condition, and  $D_0$  and  $W_0$  are the respective initial values. As we vary  $\beta$  from zero to unity, we place more emphasis on drag and less on weight. This allows us to construct Pareto fronts of optimal solutions for various geometries and gain insight into the tradeoff between weight and drag. Four values for  $\beta$  have been chosen: 0.25, 0.5, 0.75, and 1.0.

#### B. Constraints

Table 1 lists the constraints for each optimization test case considered in this study. There are two lift constraints; one corresponds to the cruise load condition, the other to a 2.5*g* load condition. Since the weight of the wing is a function of the structural thickness values, it changes over the course of the optimization. The total weight of the aircraft is assumed to be equal to the computed weight of the wing plus a fixed weight of 785,000 N. This fixed weight is estimated based on the maximum takeoff weight of a Boeing 737-900 discounted by the approximate wing weight. The approximate wing weight is equal to 7% of the maximum takeoff weight.

In practical wing design, the structures are sized based on many critical structural load conditions in order to ensure the structural integrity of the wing. The structural sizing has a profound effect on the

Table 1: Optimization constraints for all wingletted and planar cases.

Constraint	Description
Cruise	$L - W_i = 0.0$
Maneuver	$L - 2.5W_i = 0.0$
Top Skin	$KS \leq 1.0$
Bottom Skin	$KS \leq 1.0$
Rib/Spar	$KS \leq 1.0$
Total	5

Table 2: Winglet-up and winglet-down optimization design variables.

Design Variable	Quantity
Wing Sweep	1
Wing Twist	5
Wingtip Geometry	6
Section Shape	312
Angle of Attack	2
Skin Thickness	64
Spar Thickness	64
Rib Thickness	32
Total	486

aerodynamic performance of the wing. By considering a 2.5g load condition, we hope to be able to capture some of the effects of structural sizing on the tradeoff between drag and weight. This means that we must constrain the calculated stresses on the structures at the 2.5g load condition to prevent structural failure. The finite-element model of the primary wing structures used for these optimization test cases has 7,776 elements. We do not constrain each individual element’s stress value because it would require the solution to the corresponding number of coupled adjoint systems. Thus, the stresses are aggregated using the Kreisselmeier-Steinhauser (KS) technique.<sup>27,28</sup> Three KS constraints with a weighting parameter of 30 are used at the maneuver condition: one for the ribs and spars, one for the top skin, and one for the bottom skin. We use a material based on 7075 Aluminum with a Poisson’s ratio  $\nu = 0.33$  and Young’s modulus  $E = 70$  GPa. The yield stress is  $\sigma_{YS} = 434$  MPa, and a safety factor of two is applied.

### C. Design Variables

As an example, Table 2 provides a list of the design variables used for a winglet-up or winglet-down optimization case. These cases have a total of 486 design variables. There are 312 FFD control points that control the sectional shape of the wing at 26 spanwise stations. These can only move in the  $z$  direction and define the shape of the airfoil at each FFD station. Note that the control points at the wingtip (that form the 27<sup>th</sup> FFD station) do not have the freedom to control the shape of the wingtip cap, which remains fixed. This is done to avoid mesh movement failures that could otherwise occur. The structural design variables are the thickness values of the structural components, i.e. ribs, spars, and skin elements. Additional geometric design variables are the sweep and twist of the wing as well as the dihedral variables at the wingtip that allow the optimizer to develop a winglet. There are two angle of attack design variables: one for cruise, the other for the 2.5g load condition.

For the raked wingtip optimization case, the optimizer is free to manipulate a single sweep design variable that controls the raked geometry of the wingtip. As a result, this optimization case has a total of 481 design variables because there is only one geometric design variable at the wingtip. Furthermore, the planar optimization test case has a total of 480 design variables because there are no geometric design variables at the tip of the wing.

Figure 1 shows the layout of the structural components in relation to the outer mold line of the wing. The structural layout does not include the leading and trailing edges because the current model cannot accurately represent them. Figure 2 shows how both the CFD surface mesh and the structures mesh are embedded inside the FFD volume. Note that more FFD control points are clustered at the wingtip in order to allow the optimizer as much freedom as possible to develop a nonplanar feature in that region. Figure 3 shows the geometric design variables that control the shape of the wing and winglet. For a winglet-up configuration, for instance, the  $z$  coordinates of the 6 FFD stations at the wingtip are allowed to change in the positive vertical direction. This ensures that the undeflected span and planform area of the wing stay constant while allowing a winglet to form. Similarly, for a winglet-down configuration, the optimizer is free

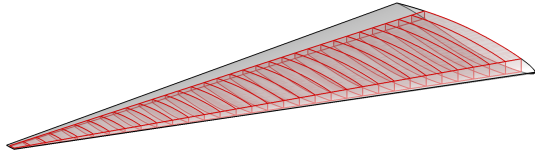
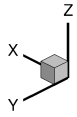


Figure 1: Primary structural layout of the wing with ribs, spars, and skin elements.

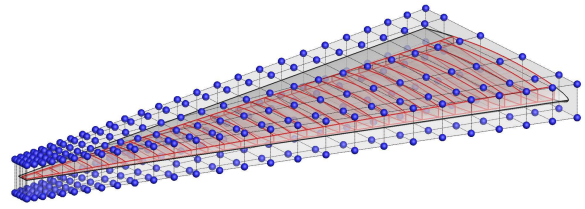
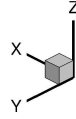


Figure 2: FFD volume around the structural and CFD meshes.

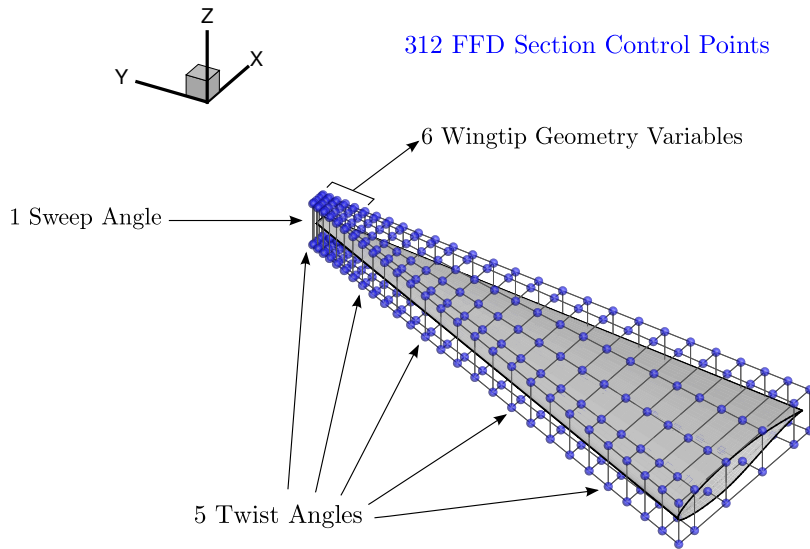


Figure 3: The geometric design variables that control the shape of the wing and winglet.

to vary the  $z$  coordinates of these stations in the negative vertical direction. The maximum height of each individual station is constrained to 10% of the span. Note that for a raked wingtip, all of these six stations are manipulated by a single sweep design variable that controls how much the tip is raked. Finally, for a planar wing optimization, these wingtip design variables are inactive.

#### D. Optimization Results

The optimization cases are performed on a CFD mesh with approximately 1.11 million nodes and a structures mesh with approximately 7,767 elements. The CFD grid does not have sufficiently fine spacings for very accurate estimations of drag. Thus, we analyze each final optimized design using a more refined CFD mesh with 58.4 million nodes in order to obtain more accurate drag estimations for the Pareto fronts. The node density of the fine grid is determined from a mesh refinement study on a sample optimized wing similar to the optimized designs presented in this paper.

As an example, Figure 4 shows the merit function history for the winglet-down configuration with  $\beta = 1.0$ . The merit function converges to the objective function value,  $J$ , when a local optimal solution that satisfies

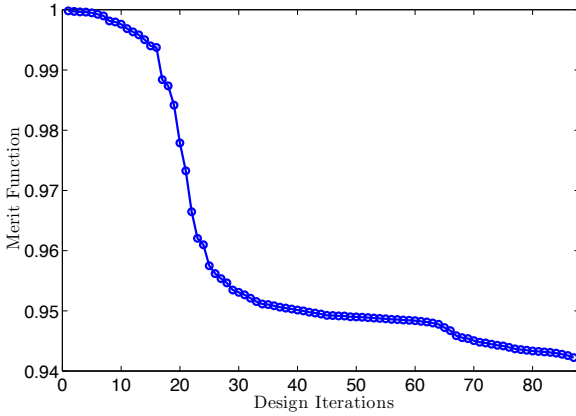


Figure 4: Merit function convergence history for the winglet-down configuration with  $\beta = 1.0$ .

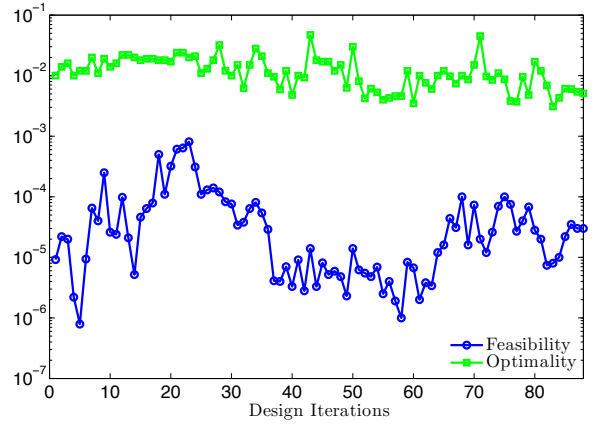


Figure 5: Feasibility and optimality convergence histories for the winglet-down configuration with  $\beta = 1.0$ .

Table 3: Aerostructural optimization results for the winglet-down configuration with  $\beta = 1.0$  at cruise.

Parameter	Value
$\alpha$	$0.75^\circ$
$C_L$	0.48
$C_{D_i}$	0.0076
Tip Deflection	5.1 ft

the nonlinear constraints is found. Figure 5 shows the corresponding convergence histories for optimality and feasibility. Optimality is a measure of the gradient of the augmented Lagrangian function used in SNOPT, and feasibility is an indicator of how well the nonlinear constraints are satisfied. We would like to see both of these measures reduced as much as possible for a well-defined local optimum. However, these aerostructural optimization cases tend to converge rather slowly.<sup>21</sup> Nevertheless, Figure 4 seems to indicate that we have obtained the majority of the objective function improvement. The optimizer completed 88 design iterations (which required 99 function evaluations) in 6 days of walltime on 256 processors. These general convergence trends hold true for the rest of the optimization cases as well. Table 3 lists a few important parameters for the optimized winglet-down design with  $\beta = 1.0$  at the cruise condition.

We chose not to include results for  $\beta = 0.0$ . With  $\beta = 0.0$ , the objective function is equal to the normalized weight of the wing. Since the quarter-chord sweep angle of the wing is a geometric design variable, the optimizer reduces the sweep as much as possible in order to take advantage of the corresponding reduction in the structural weight. This leads to designs that have relatively strong shocks on both the upper and lower surfaces of the wing because the resultant increase in wave drag is not reflected in the objective function. As a result, these optimization cases are particularly difficult to converge and require many more function evaluations to reach an acceptable convergence level. However, there are no such difficulties with  $\beta = 1.0$ . When the objective function is purely the normalized inviscid drag of the wing, the optimizer does not increase the sweep angle to the upper bound. The reason is that while increasing the sweep angle helps reduce the drag, a highly swept-back wing will be heavy and, as a result, it will have to produce a large amount of lift. This will lead to a large amount of lift-induced drag which in turn results in an increase in the objective function.

Figure 6 shows the contours of pressure coefficient on the top surface for the winglet-down configuration with  $\beta = 1.0$ . The corresponding structural thickness values are also shown. Note that the aerostructural optimization has thickened the skin inboard. This is somewhat expected because the failure criterion at the 2.5g load condition tends to be closer to the critical value at the root of the wing. Although we have not

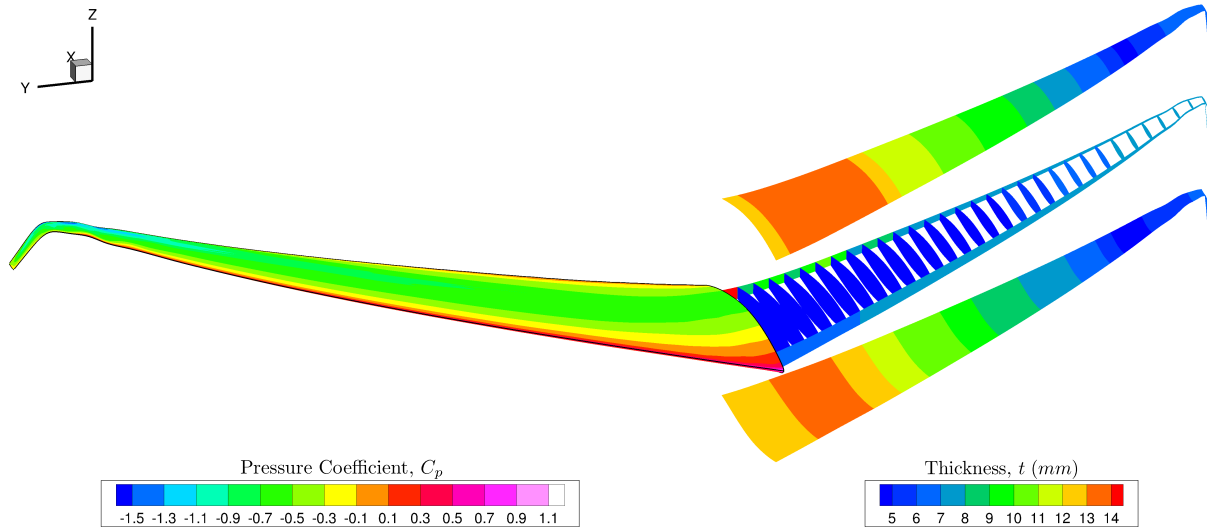


Figure 6: Contours of pressure coefficient on the top surface (left) and structural thickness values in millimeters (right) for the winglet-down configuration with  $\beta = 1.0$ .

considered all of the necessary critical load conditions that are required in the context of wing design, this result shows that we are likely to capture at least some of the correct trends dictated by the structural sizing of the wing.

As an example, Figure 7 shows the spanwise lift distributions for the cruise and 2.5g load conditions corresponding to the planar wing configuration with  $\beta = 0.5$ . These have been normalized with respect to the lift at the root for an elliptical lift distribution at cruise. It is important to note that the optimizer is aeroelastically tailoring the wing in order to significantly reduce the tip loading at the 2.5g load condition while maintaining an optimal lift distribution for the planar wing at the cruise condition.

Figure 8 shows the weight and inviscid drag performance of the optimized winglet configurations and the optimized planar wing obtained with  $\beta = 0.5$ . All weight, drag, and objective function values are normalized by those of the optimized planar wing. Thus, the weight, drag, and objective function values of the optimized planar wing are equal to unity. The black line in this figure encompasses all of the designs that would have an objective function value equal to that of the optimized planar wing. Any point below this line has a lower objective function value than the optimized planar design. Conversely, any point above this line has a higher objective function value than the optimized planar wing. This is further demonstrated by a colorbar where the color of each point is related to its objective function value. Note that all of the optimization cases presented in this paper use the same initial planar design, which is *not* shown on this figure. The initial design satisfies all of the nonlinear constraints to a tolerance of  $10^{-5}$ . The exact values of the objective function and the span efficiency factor (defined as  $e = L^2/\pi q_\infty b^2 D$ ) for each point along with the corresponding deflected shape are also shown for clarity. The optimizer reduces the strength of shock waves as much as possible using the sectional shape design variables and sweep. Thus, wave drag is minimized and, as a result, the span efficiency factor can be used to compare the inviscid drag performance of the wingletted wings in comparison to the planar wing.

Figure 8 demonstrates that the winglet-down configuration is the most competitive design when  $\beta = 0.5$ . Although it has the highest weight, it is providing an improved inviscid drag performance in comparison to all of the other configurations. The inviscid drag of the winglet-down configuration is almost 5% lower than the optimized planar wing. Most importantly, its objective function value is approximately 2% lower than that of the planar wing. Furthermore, at the deflected state of the wing, it has the highest span. The reader may recall from Section III that the undeflected spans of all of the configurations considered in this

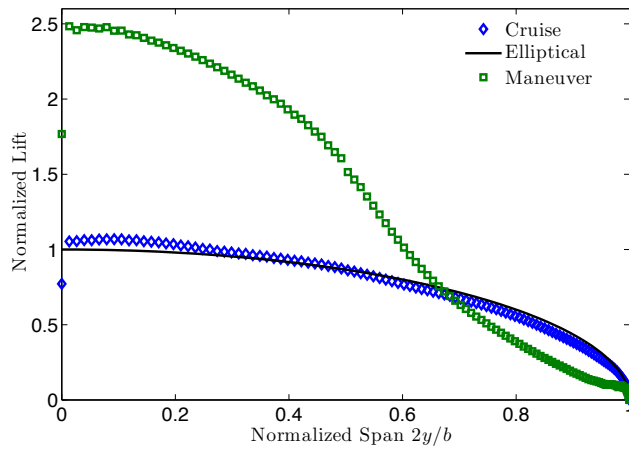


Figure 7: Spanwise lift distributions at the cruise and 2.5g load conditions for the planar configuration with  $\beta = 0.5$ .

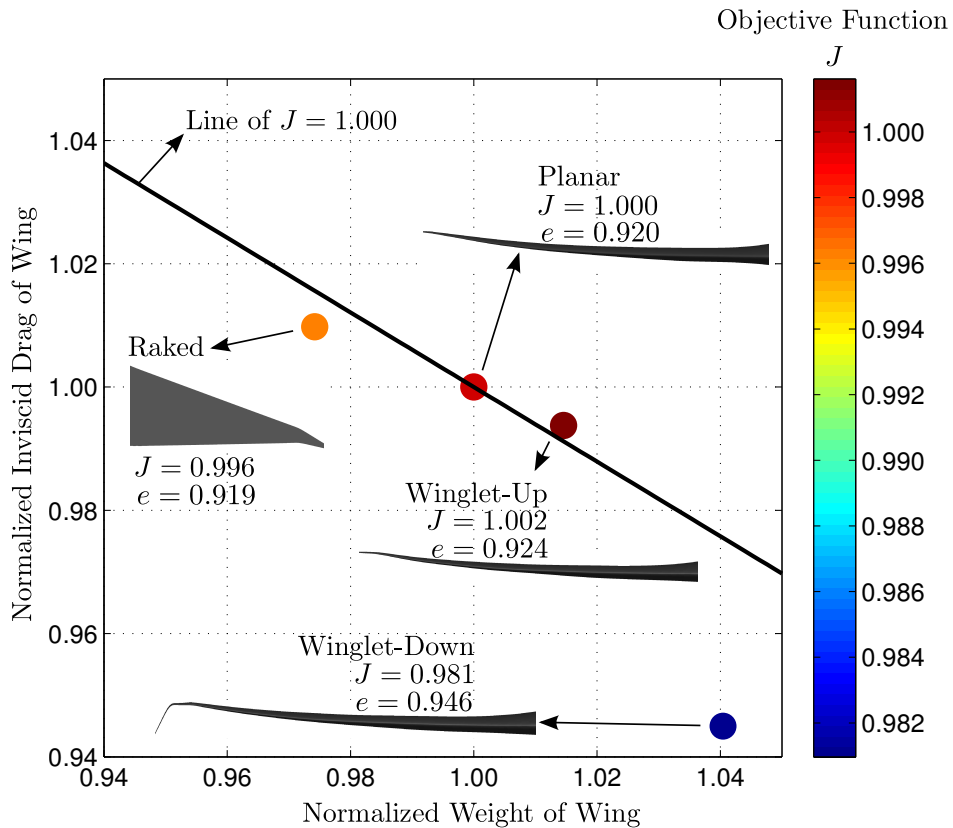


Figure 8: Weight and inviscid drag performance of the optimized winglet configurations in relation to the optimized planar wing obtained with  $\beta = 0.5$ .

study are the same. However, the spans may be different at the deflected state of the wings, especially in the presence of a winglet. This is further illustrated in Figures 9 and 10. Since the winglet-down configuration has the longest span, it delivers an improved induced drag performance in comparison to the rest of the configurations shown in Figure 8. This is a subtle effect, but it reveals an interesting point: the optimizer is taking advantage of the changes in the deflected shape of the wings. This is accomplished by manipulating the sectional shape, twist, and structural thickness design variables that control the deflected shape of the

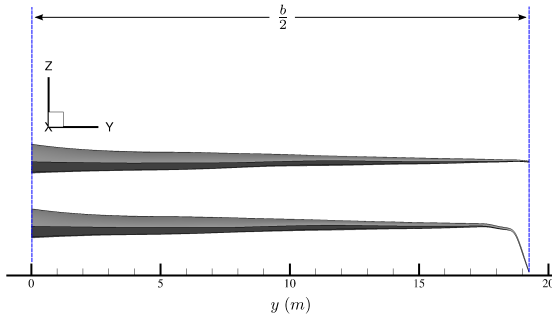


Figure 9: The undeformed shapes of the winglet-down and planar configurations with  $\beta = 0.5$ . The spans are exactly equal.

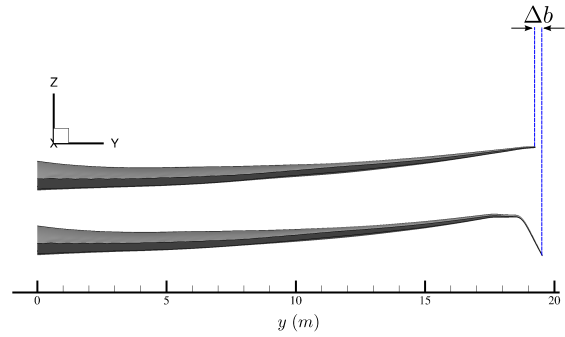


Figure 10: The deflected shapes of the winglet-down and planar configurations in cruise with  $\beta = 0.5$ . The deflected spans are different.

wing under the cruise aerodynamic loads.

An important point that deserves the reader’s attention is that the winglet-up, raked wingtip, and planar configurations have almost the same objective function value. Although there are differences in terms of their relative inviscid drag and weight performance, none of them is at an advantage against any other because all three designs practically fall on the line of  $J = 1.0$ .

The winglet-up configuration shown in Figure 8 is almost identical in shape to the planar wing. Although the values of the winglet design variables at the tip of the winglet-up configuration are nonzero, they are small relative to the span. Thus, it is important to note that the optimizer kept the wingtip almost planar even though it did have the freedom to generate a conventional winglet. One reason the optimizer chose not to create a well-pronounced blended winglet might be that such a design could have a lower deflected span.

Although the winglet-down configuration appears to be the most competitive design with  $\beta = 0.5$ , i.e. when equal emphasis is placed on inviscid drag and weight in the objective function, its relative benefit in comparison to the planar wing can be within the uncertainties in the models used. Furthermore, our results seem to indicate that the induced drag advantage of the winglet-down configuration is due to the increased span of the wing at the deflected state and is less than the improvement reported by Hicken and Zingg<sup>12</sup> for a low-speed, rectangular wing. We already saw in Figure 8 that within the capabilities of our framework, the rest of the wingletted wings also do not seem to provide a substantial performance improvement as compared to the optimized planar wing. This suggests that perhaps we should include other phases of a commercial flight profile such as the steady climb where the  $C_L$  is higher and, as a result, the induced drag is larger than it is in cruise.

Figure 11 shows the Pareto front of optimal designs for weight and drag for the winglet-down configuration. The weight and drag values shown are normalized by the highest values of weight and drag, respectively. Note that for the purpose of this plot, the weight values are obtained by adding the calculated wing weight to a fixed weight of 785,000 N to get an approximate total aircraft weight. Similarly, the drag values are obtained by adding the calculated inviscid drag based on the Euler equations to a friction drag estimation of the aircraft. This friction drag estimation method is based on the exposed area of the fuselage, wing, and tail,<sup>33</sup> and is used here only to penalize the designs with larger surface area. The friction drag estimation is not included in the objective function for the purpose of optimization. The values of  $\beta$  along with a view of the optimal wing shapes at their deflected state are also provided. As the value of  $\beta$  increases from 0.25 to 1.0, i.e. as we place increasing emphasis on the drag in the objective function, the drag values of the optimal shapes decrease at the cost of increasing the weight. This is the expected trend for this particular family of objective functions. An interesting aspect of this plot is the fact that the winglet-down feature becomes more pronounced when  $\beta$  increases from 0.25 to 0.50. This is reasonable because as we place more emphasis on drag in the objective function, the optimizer takes more advantage of the nonplanar feature at the tip to decrease induced drag. Although not shown on this plot, the quarter-chord sweep angles of the wings also

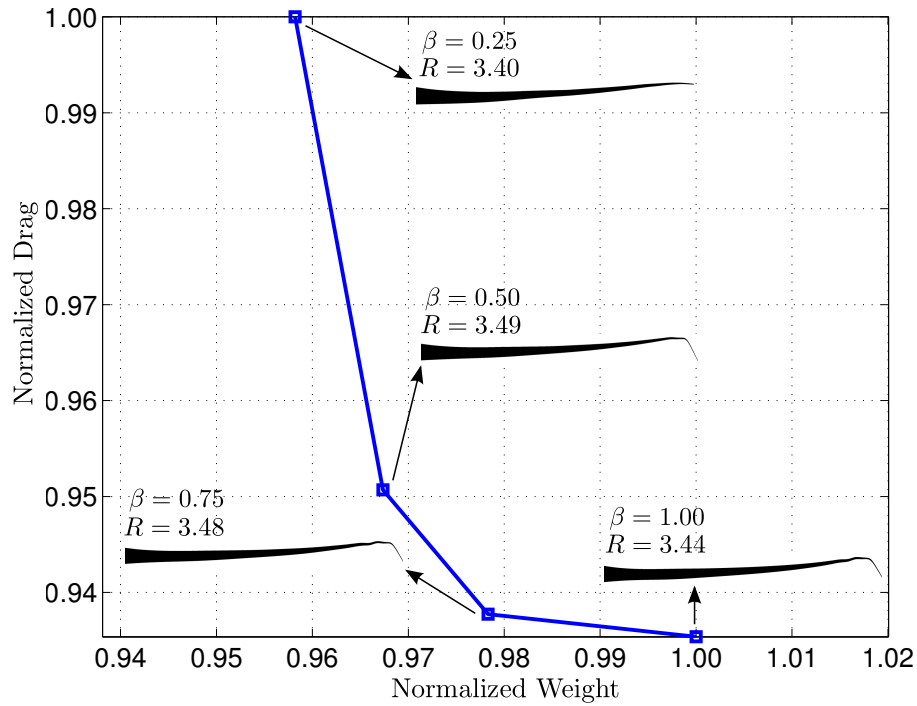


Figure 11: Pareto front of optimal designs for the winglet-down configurations.

increase with increasing  $\beta$  because wing sweep helps reduce wave drag.

Figure 11 also shows a range parameter for each of the optimal solutions that is of the form

$$R = \frac{C_L}{C_D} \ln \frac{W_i}{W_f} \quad (2)$$

where  $C_L$  is the lift coefficient,  $C_D$  is the drag coefficient including the friction drag estimation for the aircraft,  $W_i$  is the initial weight, and  $W_f$  is the final weight of the aircraft. The difference between the initial and final weights,  $W_i - W_f$  is equal to the approximate fuel weight, which is assumed to be 206,000 N. Note that velocity and thrust specific fuel consumption do not appear in Equation 2 because the operating velocity and engine parameters are assumed constant. Thus, the interdisciplinary effects of the propulsion system on range are ignored. Furthermore, skin friction drag is not included in the objective function for the purpose of optimization and, as a result, the aerostructural tradeoff between the lift-to-drag and weight ratios in Equation 2 is not a perfect reflection of the correct tradeoff in the context of practical aircraft design. Hence, we cannot draw firm conclusions about the variation in  $R$  with  $\beta$  from these results alone, but it is interesting to note that the maximum  $R$  value is attained when there is equal emphasis on weight and drag in the objective function.

Figure 12 shows the Pareto fronts of optimal solutions obtained for all of the configurations considered in this study. The optimized planar wing with  $\beta = 0.25$  has a normalized drag value equal to unity. Similarly, the optimized planar wing with  $\beta = 1.0$  has a normalized weight value equal to unity. This normalization is done in order to make the comparison between the wingletted and planar wings easier. Note that the actual weight and drag values on this plot also include the fixed mass and the friction drag estimation that was previously mentioned.

In all cases, as we place increasing emphasis on inviscid drag in the objective function, i.e. as we vary  $\beta$  from 0.25 to 1.0, the drag decreases at the cost of increasing weight. Figure 12 also shows that the winglet-down configuration is competitive for all objective functions with the exception of the  $\beta = 0.25$  case. The improved drag performance is due to the increased deflected span of this configuration under the cruise

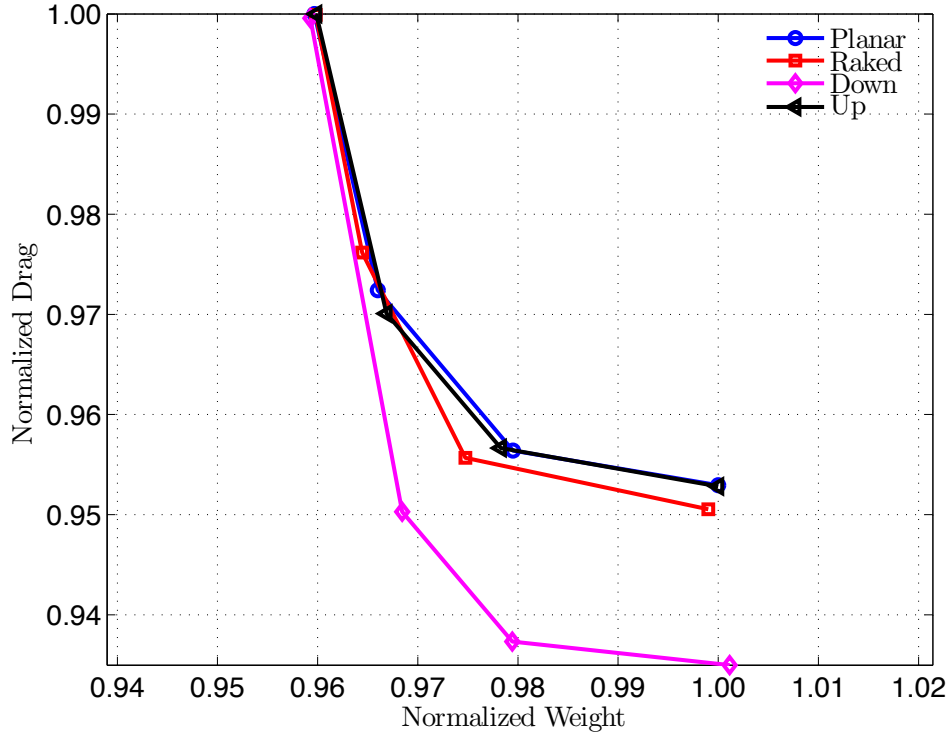


Figure 12: Pareto fronts of optimal designs for all of the wingletted and planar configurations considered in this study.

aerodynamic loads. However, the drag reduction is at best only 2%. Furthermore, the Pareto fronts for the rest of the wingletted wings lie very close to that of the planar configurations. Thus, the most important conclusion obtained from Figure 12 is that the presence of a nonplanar wingtip does not seem to significantly change the fundamental tradeoff between drag and weight in the context of this particular class of design problems. Moreover, we have ignored the effects of viscosity in our optimizations, but they have important implications for the design of wings with winglets.

#### IV. Conclusions

Aerostructural optimization based on the Euler equations has been applied to a family of optimization cases in order to understand the fundamental tradeoffs between drag and weight in the design of wings with winglets. Pareto fronts of optimal designs are constructed by minimizing the sum of the normalized weight and inviscid drag of the wings with varying emphasis on weight and drag. The configurations considered in this study are winglet-up, winglet-down, and raked wingtips. These are compared to optimized planar wings with the same undeflected span. Our results indicate that the winglet-down configuration is the most competitive design, except in the case where there is more emphasis on weight than on drag. The larger span of the wings at the deflected state under the cruise aerodynamic loads appears to be responsible for the improved induced drag performance of this configuration. The inviscid drag benefit provided by the winglet-down configuration is around 5%. When a friction drag estimation of the aircraft based on surface area is included, the drag improvement of the winglet-down configuration is approximately 2%. Future work will focus on investigating the potential of wings with winglets for drag reduction in other phases of a commercial flight profile, such as the steady climb, where the induced drag is large.

## Acknowledgments

The authors are thankful to Prof. Joaquim R. R. A. Martins of the University of Michigan, Ann Arbor for sharing his software and methodology for the purpose of constructing our framework. Furthermore, this work would not have been possible without the contributions of Ms. Jenny Z. Zhang of the University of Toronto Institute for Aerospace Studies. Finally, the authors gratefully acknowledge the financial support provided by the Ontario Graduate Scholarship program and the University of Toronto. Computations were performed on the GPC supercomputer at the SciNet HPC Consortium. SciNet is funded by: the Canada Foundation for Innovation under the auspices of Compute Canada, the Government of Ontario, Ontario Research Fund - Research Excellence, and the University of Toronto.

## References

- <sup>1</sup>Kroo, I., "Drag Due to Lift: Concepts for Prediction and Reduction," *Annual Review of Fluid Mechanics*, Vol. 33, No. 1, 2001, pp. 587-617.  
doi: 10.1146/annurev.fluid.33.1.587
- <sup>2</sup>Whitcomb, R., "A Design Approach and Selected Wind Tunnel Results at High Subsonic Speeds for Wing-Tip Mounted Winglets," NASA, TN-D-8260, 1976.
- <sup>3</sup>Heyson, H. H., Riebe, G. D., and Fulton, C. L., "Theoretical Parametric Study of the Relative Advantages of Winglets and Wing-Tip Extensions," NASA, TP-1020, 1977.
- <sup>4</sup>Jones, R. T., and Lasinsky, T. A., "Effects of Winglets on the Induced Drag of Ideal Wing Shapes," NASA, TM-81230, 1980.
- <sup>5</sup>Asai, K., "Theoretical Considerations in Aerodynamic Effectiveness of Winglets," *Journal of Aircraft*, Vol. 22, No. 7, 1985, pp. 635-637.  
doi: 10.2514/3.45177
- <sup>6</sup>Van Dam, C. P., "Induced-Drag Characteristics of Crescent-Moon-Shaped Wings," *Journal of Aircraft*, Vol. 24, No. 2, 1987, pp. 115-119.  
doi: 10.2514/3.45427
- <sup>7</sup>Smith, S. C., and Kroo, I. M., "Computation of Induced Drag for Elliptical and Crescent-Shaped Wings," *Journal of Aircraft*, Vol. 30, No. 4, 1993, pp. 446-452.  
doi: 10.2514/3.46365
- <sup>8</sup>Takenaka, K., and Hatanaka K., "Multidisciplinary Design Exploration for a Winglet," *Journal of Aircraft*, Vol. 45, No. 5, 2008, pp. 1601-1611.  
doi: 10.2514/1.33031
- <sup>9</sup>Verstraeten, J. G., and Slingerland, R., "Drag Characteristics for Optimally Span-Loaded Planar, Wingletted, and C Wings," *Journal of Aircraft*, Vol. 46, No. 3, 2009, pp. 962-971.  
doi: 10.2514/1.39426
- <sup>10</sup>Ning, S. A., and Kroo, I., "Multidisciplinary Considerations in the Design of Wings and Wing Tip Devices," *Journal of Aircraft*, Vol. 47, No. 2, 2010, pp. 534-543.  
doi: 10.2514/1.41833
- <sup>11</sup>Jansen, P. W., Perez, R. E., and Martins, J. R. R. A., "Aerostructural Optimization of Nonplanar Lifting Surfaces," *Journal of Aircraft*, Vol. 47, No. 5, 2010, pp. 1490-1504.  
doi: 10.2514/1.44727
- <sup>12</sup>Hicken, J. E., and Zingg, D. W., "Induced-Drag Minimization of Nonplanar Geometries Based on the Euler Equations," *AIAA Journal*, Vol. 48, No. 11, 2010, pp. 2564-2575.  
doi: 10.2514/1.J050379
- <sup>13</sup>Gagnon, H., and Zingg, D. W., "High-fidelity Aerodynamic Shape Optimization of Unconventional Aircraft through Axial Deformation," *52nd Aerospace Sciences Meeting, AIAA SciTech*, AIAA-2014-0908, National Harbor, MD, January 2014.  
doi: 10.2514/6.2014-0908
- <sup>14</sup>Hicken, J. E., and Zingg, D. W., "A Parallel Newton-Krylov Solver for the Euler Equations Discretized Using Simultaneous Approximation Terms," *AIAA Journal*, Vol. 46, No. 11, 2008, pp. 2773-2786.  
doi: 10.2514/1.34810
- <sup>15</sup>Osusky, M., and Zingg, D. W., "A Parallel Newton-Krylov-Schur Flow Solver for the Reynolds-Averaged Navier-Stokes Equations," *50th AIAA Aerospace Sciences Meeting and Exhibit*, AIAA-2012-0442, Nashville, TN, January 2012.  
doi: 10.2514/6.2012-442
- <sup>16</sup>Kennedy, G. J., and Martins, J. R. R. A., "Parallel Solution Methods for Aerostructural Analysis and Design Optimization," *13th AIAA/ISSMO Multidisciplinary Analysis Optimization Conference*, AIAA-2010-9308, Fort Worth, TX, September 2010.  
doi: 10.2514/6.2010-9308
- <sup>17</sup>Leung, T. M., Zingg, D. W., "Aerodynamic Shape Optimization of Wings Using a Parallel Newton-Krylov Approach," *AIAA Journal*, Vol. 50, No. 3, 2012, pp. 540-550. doi: 10.2514/1.J051192
- <sup>18</sup>Kenway, G. K. W., Kennedy, G. J., and Martins, J. R. R. A., "A CAD-Free Approach to High-Fidelity Aerostructural Optimization," *13th AIAA/ISSMO Multidisciplinary Analysis Optimization Conference*, AIAA-2010-9308, Fort Worth, TX, September 2010.  
doi: 10.2514/6.2010-9231

- <sup>19</sup>Gill, P. E., Murray, W., and Saunders, M. A., “SNOPT: An SQP Algorithm for Large-Scale Constrained Optimization,” *Society for Industrial Applied Mathematics Review*, Vol. 47, No. 1, 2005, pp. 99-131.  
doi: 10.1137/S0036144504446096
- <sup>20</sup>Perez R. E., Jansen P. W., and Martins J. R. R. A., “pyOpt: A Python-Based Object-Oriented Framework for Nonlinear Constrained Optimization,” *Structures and Multidisciplinary Optimization*, Vol. 45, No. 1, 2012, pp. 101-118.  
doi: 10.1007/s00158-011-0666-3
- <sup>21</sup>Kenway, G. K. W., Kennedy, G. J., and Martins, J. R. R. A., “Scalable Parallel Approach for High-Fidelity Steady-State Aeroelastic Analysis and Adjoint Derivative Computations,” *AIAA Journal*, Vol. 52, No. 5, pp. 935-951.  
doi: 10.2514/1.J052255
- <sup>22</sup>Leung, T. M., Zhang, J., Kenway, G. K. W., Kennedy, G. J., Wang, X., Zingg, D. W., Martins, J. R. R. A., “Aerostructural Optimization Using a Coupled-Adjoint Approach,” *Canadian Aeronautics and Space Institute 60th Aeronautics Conference and Annual General Meeting*, Toronto, ON, May 2013.
- <sup>23</sup>Zingg, D. W., Nemec, M. A., and Pulliam, T. H., “A Comparative Evaluation of Genetic and Gradient-Based Algorithms Applied to Aerodynamic Optimization,” *European Journal of Computational Mechanics*, Vol. 17, No. 1, 2008, pp. 103-126.
- <sup>24</sup>Chernukhin, O., and Zingg, D. W., “Multimodality and Global Optimization in Aerodynamic Design,” *AIAA Journal*, Vol. 51, No. 6, 2013, pp. 1342-1354.  
doi: 10.2514/1.J051835
- <sup>25</sup>Martins, J. R. R. A., Alonso, J. J., and Reuther, J. J., “A Coupled-Adjoint Sensitivity Analysis Method for High-Fidelity Aero-Structural Design,” *Optimization and Engineering*, Vol. 6, No. 1, 2005, pp. 33-62.  
doi: 10.1023/B:OPTE.0000048536.47956.62
- <sup>26</sup>Kroo, I., “Aircraft Design: Synthesis and Analysis,” March 2014, URL <http://adg.stanford.edu/aa241/AircraftDesign.html>.
- <sup>27</sup>Akgün, M. A., Haftka, R. T., Wu, K. C., Walsh, J. L., and Garcelon, J. H., “Efficient Structural Optimization for Multiple Load Cases Using Adjoint Sensitivities,” *AIAA Journal*, Vol. 39, No. 3, 2001, pp. 511-516.  
doi: 10.2514/2.1336
- <sup>28</sup>Poon, N. M. K., and Martins, J. R. R. A., “An adaptive approach to constraint aggregation using adjoint sensitivity analysis,” *Structural and Multidisciplinary Optimization*, Vol. 30, No. 1, 2007, pp. 61-73.  
doi: 10.1007/s00158-006-0061-7
- <sup>29</sup>Reist, T. A., and Zingg, D. W., “Aerodynamic Shape Optimization of a Blended-Wing-Body Regional Transport for a Short Range Mission,” *31st Applied Aerodynamics Conference*, AIAA-2013-2414, San Diego, CA, June 2013.  
doi: 10.2514/6.2013-2414
- <sup>30</sup>Hicken, J. E., and Zingg, D. W., “Aerodynamic Optimization Algorithm with Integrated Geometry Parameterization and Mesh Movement,” *AIAA Journal*, Vol. 48, No. 2, 2010, pp. 401-413.  
doi: 10.2514/1.44033
- <sup>31</sup>Osusky, L., and Zingg, D. W., “A Novel Aerodynamic Shape Optimization Approach for Three-Dimensional Turbulent Flows,” *50th AIAA Aerospace Sciences Meeting and Exhibit*, AIAA-2013-0058, Nashville, TN, January 2012.  
doi: 10.2514/6.2012-58
- <sup>32</sup>Kuntawala, N. B., Hicken, J. E., and Zingg, D. W., “Preliminary Aerodynamic Shape Optimization of a Blended-Wing-Body Aircraft Configuration,” *49th AIAA Aerospace Sciences Meeting and Exhibit*, AIAA-2013-0058, Orlando, FL, January 2011.  
doi: 10.2514/6.2011-642
- <sup>33</sup>Raymer, D. P., “Aircraft design: a conceptual approach,” *Aerodynamics*, 5th ed., AIAA Education Series, AIAA, Virginia, 2012, pp. 429-430.